

A computer vision system for oocyte counting using images captured by smartphone

Celso Soares Costa^{a,d,*}, Everton Castelão Tetila^{b,d}, Gilberto Astolfi^{a,c}, Diego André Sant'Ana^{a,d}, Marcio Carneiro Brito Pacheco^{a,d}, Ariadne Barbosa Gonçalves^c, Vanda Alice Garcia Zanoni^{e,d}, Higor Henrique Picoli Nucci^c, Odair Diemer^a, Hemerson Pistori^{d,c}

^a Federal Institute of Education, Science and Technology of Mato Grosso do Sul, Mato Grosso do Sul, Campo Grande, Brazil

^b Federal University of Grande Dourados, Dourados, Mato Grosso do Sul, Brazil

^c Federal University of Mato Grosso do Sul, Campo Grande, Mato Grosso do Sul, Brazil

^d Dom Bosco Catholic University, Campo Grande, Mato Grosso do Sul, Brazil

^e Brasília University, Brasília, Federal District, Brazil

ARTICLE INFO

Keywords:

Computer vision
Fish reproductive process
Fish oocyte count
Smartphone images
Astyanax bimaculatus

ABSTRACT

This work proposes a computer vision procedure for counting Twospot astyanax (*Astyanax bimaculatus*) oocytes in Petri dishes using images captured by smartphone. First, the proposed procedure uses simple linear iterative clustering (SLIC) to divide the images into groups of pixels (superpixels). Then, based on their color and space characteristics, the images are classified into light background, dark background, dirt, or oocyte by a machine learning algorithm. Five different types of machine learning algorithms were tested: support vector machines (SVM), decision trees using the algorithm J48 and random forest, *k*-nearest neighbors (*k*-NN), and Naive Bayes. To train the algorithms, 8,578 superpixels were classified by an expert into oocyte ($n = 354$), dirtiness ($n = 651$), dark background ($n = 3,622$), and light background ($n = 3,951$). Of the five learning algorithms, SVM obtained the best result with 97% correct oocyte recognition. Given the wide availability of smartphones, we therefore conclude that the presented procedure can be a valuable tool in future experiments and studies on fertilization and hatching success in Twospot astyanax.

1. Introduction

According to the United Nations Food and Agriculture Organization (FAO) (FAO, 2018), aquaculture is the fastest growing food sector in the world, and world fish consumption rose to 20.3 kg/capita/year in 2016, above 9 kg/capita/year in 1961. Brazil is one of the few countries with aquatic environments available for the sustainable development of aquaculture (Kirchner et al., 2016).

For the success of aquaculture, it is important that fish species reproduce with maximum efficiency (Santín et al., 2010). The artificial reproduction of native fish used in Brazil is common, call of hypophy-sation. This the most used method in breeding farms and is based on hormonal dose applications (Kirchner et al., 2016; Santín et al., 2010). In this technique, the measurement and counting of fish oocytes is a very laborious, tedious, time-consuming, and stressful activity, performed manually by means of a stereoscopic to amplify the visual observation, and requires an experienced professional. This fatigue can lead to failures that can compromise the reproductive process (Ganias,

2013; Shimoda et al., 2007; Bittencourt et al., 2018).

According to Duan et al. (2015), automatic counting systems for fish oocytes decrease the human working time when compared to traditional manual counting methods. Moreover, computer vision has several advantages: it results in simple and fast processes, speeds up the visual analysis, has high reliability, and, unlike the human eye, it never becomes tired. It also has good accuracy, a wide range of use, and low cost. Finally, computer vision is easy to use and is compatible with mobile devices (Singh and Kumar, 2016; Parashar and Parashar, 2017).

According to Singh and Kumar (2016), mobile smartphones with cameras have become widely available and have already been proven suitable for several image analysis applications. The United Nations Development Program reported (UNDP, 2015) that Brazil has 117 cell phones per 100 people, and 60.9% of the population has access to the Internet. Therefore, the advancement of electronic technology makes the smartphone suitable for performing image processing techniques, and the data can be applied to productivity estimates (Gong et al., 2013). Zhang et al. (2017) believe that computer vision researchers are

* Corresponding author at: Federal Institute of Education, Science and Technology of Mato Grosso do Sul, Mato Grosso do Sul, Campo Grande, Brazil.

E-mail address: celso.costa@ifms.edu.br (C.S. Costa).

enthusiastic about the possibility of using mobile devices for data capture and processing.

In this context, the present study proposes a procedure for the automatic counting of lambari oocytes *Astyanax bimaculatus* using machine learning from images captured by a smartphone.

We considered an image segmentation step based on the simple linear iterative clustering (SLIC) method to detect fish oocytes in a Petri dish. We described the segments using combined attribute extractors based on visual characteristics has been tested using color, gradient, texture, and shape.

The proposed approach was tested using a set of 8.578 images and 395 attributes. Based on the set, four classes were determined (oocyte, light background, dark background, and dirtiness) to evaluate five well-known classifiers from the literature in the task of oocyte recognition and counting.

2. Materials and methods

2.1. Proposed approach

We present a computational vision approach to count lambaris oocytes through images collected by a smartphone. Fig. 1 presents the steps of the proposed system in a schematic diagram. This illustrates the methodology, which consists of five steps: (a) acquisition of images with a smartphone, (b) segmentation using SLIC and superpixel annotation, (c) attribute extraction, and (d) classification of oocyte counts.

The initial step is the acquisition/capture process of the smartphone images of a Petri dish during the breeding process, as illustrated in Fig. 1(a). These images were segmented using the SLIC superpixel method. The proposed approach adopts the SLIC.

The SLIC is an algorithm (Achanta et al., 2012) that groups similar image pixels into atomic regions, creating a superpixel. The strategy of SLIC groups pixels based on color similarities and spatial proximities in the image. The algorithm receives as input a K value that represents the number of superpixels to get from the image. Then, the SLIC defines K cluster centers, i.e., K superpixel centers. Cluster centers are distributed across the grid image, and in an iterative process, SLIC calculates the proximity of each image pixel to each cluster center using a measurement based on color and spatial distance. Then, the pixels are grouped around their nearest cluster center, forming superpixels. Each superpixel extracted from the image is visually classified into four specific classes in such a way that the raw material of the collected sample can be characterized.

After segmenting the image with the SLIC method, the segments were classified and visually annotated by a professional expert to compose a training set and subsequently test the system (see step (b) of Fig. 1). Subsequently, the images were described based on color, gradient, texture, and shape characteristics automatically extracted from each superpixel (see step (c) of Fig. 1). Finally, the information was submitted to machine learning algorithms.

In supervised learning, a model is trained/fed with sample data that is labeled with the desired outputs. In this method, the algorithm is able to learn to find errors and modify the model accordingly. Supervised

learning, therefore, uses pattern recognition to predict label values in additional nonlabeled data. Using Weka software 3.6.14 (Hall et al., 2009), experiments were conducted with supervised learning techniques called classification algorithms.

The final step of the computer vision system shows the visual and quantitative results by classifying the segments of a Petri dish image according to predefined classes [Fig. 1(d)]. The oocyte counting is a trial-by-product of superpixel classification, as now we just need to add all superpixels classified as oocytes.

2.2. Location of experimental environment

The research was carried out in the state of Mato Grosso do Sul-MS in partnership with the Federal Institute of Education Science and Technology of Mato Grosso do Sul (IFMS) and Dom Bosco Catholic University. The images of the lambari oocytes were captured with a smartphone during a breeding process in December 2017 in the laboratory of IFMS (Fig. 2) located on the Coxim-MS campus. All procedures involving animals were conducted according to standards approved by the IFMS Animal Ethics Committee.

2.3. Lambari reproduction

Six funnel-type incubators with 200l of water were used to reproduce lambari. In each incubator, a galvanized steel samburá 5, no. 0, with a width of 19 cm and height of 30 cm was placed to pick up the eggs. The fish (male and female) were submitted to the traditional hypophysis protocol and inserted in the samburás. After spawning, the fish were removed, leaving only the eggs in the incubators. We used 120 males with an average weight of 10.63 g and an average length of 8.30 cm, and 60 females with an average weight of 20.17 g and an average length of 11.00 cm. In each incubator, 20 males and 10 females were placed. At spawning, the eggs were temporarily removed from the incubators to be counted.

2.4. Image acquisition

The acquisition of images was done in a semicontrolled environment in.JPG format with a quality (compression) level of 93% using Asus ZenFone 2 ZE551ML 1.8 GHz, Android 4.0, 5.5, 16 GB memory with a camera resolution of 4096×2304 pixels (equivalent to 13 megapixels). The images were captured at a distance of approximately 10 cm above the Petri dish without using a flash and smartphone zoom. A blank sheet of paper was placed under the Petri dish so that its transparent surface did not reveal the dish support base. To allow for a clear and uniform visualization of the bottom of the Petri dish, a 100-mm polyvinyl chloride (PVC) light tube supported the Petri dish.

2.5. Visual analysis and SLIC segmentation

In analyzing the images of the Petri dish with a sample of oocytes, regions were identified and classified as shown in Fig. 3. In the dish, there was no presence of overlapping oocytes, i.e., there was a

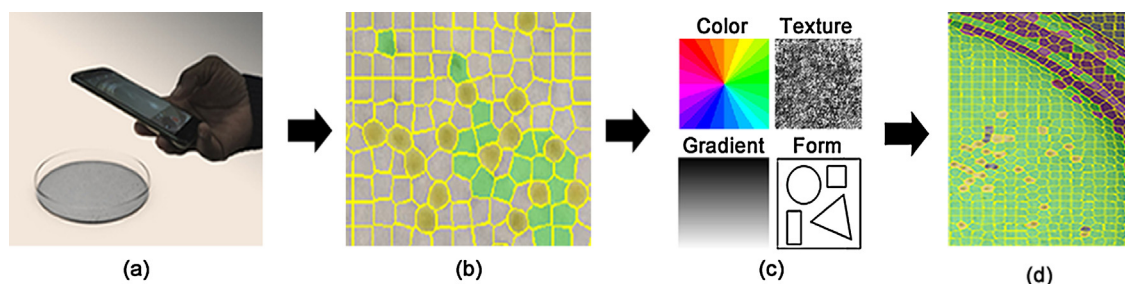


Fig. 1. Proposed steps of computer vision system for oocyte counting with smartphone images.

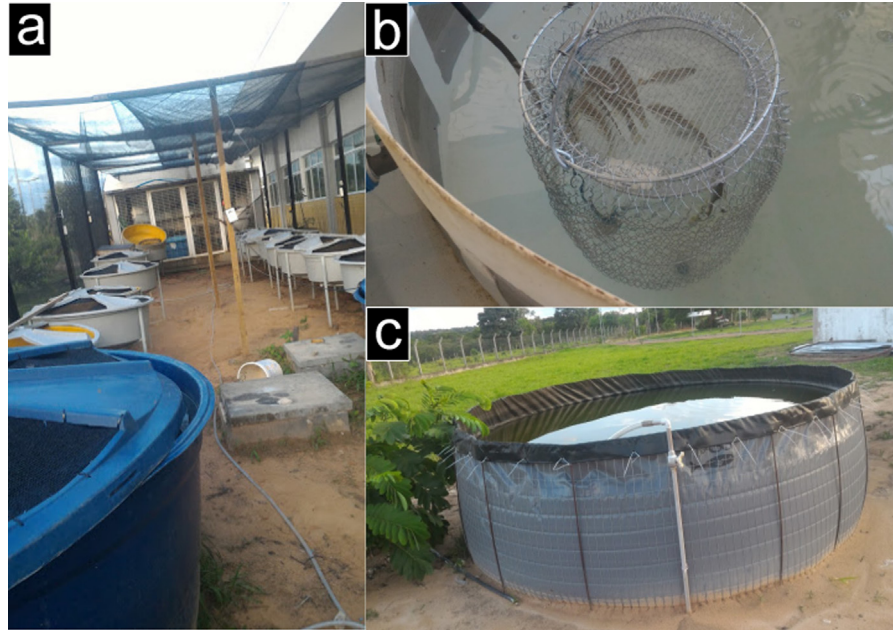


Fig. 2. Laboratory of reproduction and larviculture of native fish: (a) laboratory with 20 boxes of water with capacity of 250 l for larviculture and six incubators for hatching of eggs, (b) details of incubator with lambaris inside samburá for natural spawning, and (c) geomembrane tank where matrices were maintained.

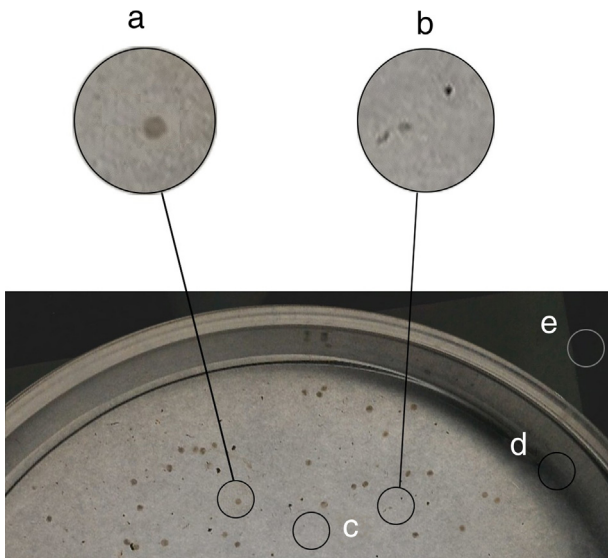


Fig. 3. Representation of regions and classes in image of Petri dish: (a) oocyte, (b) dirtiness, (c) light background, (d) and (e) dark background.

maximum of one oocyte per superpixel segment. We used this class to count the oocytes. The enlargement in Fig. 3(a) indicates the region of the image with an oocyte.

Dirtiness, as shown in Fig. 3(b), indicates a region in which small fragments were found. These fragments include plant remains, bark, leaves, and even parts of the body of the fish, which are common occurrences in aquatic environments. Fig. 3(c) illustrates the light background class. This region shows an intensification of ambient light. However, the dark background class, shown in Fig. 3(d) and (e), occurs because of the absence of light or the presence of shadows on the Petri dish.

To identify the oocytes in the Petri dish, each image was segmented by the superpixel-based method according to the parameter K that best adjusts the detection of the oocyte areas in the Petri dish image.

In the classification task, we submitted the captured images to the machine learning models. Initially, the experiment strove to find the best parameter of K . This was done empirically using a value of K equal to 190 and 250. Then, this value was increased several times to $K = 16,000$, corresponding to the mean area of an oocyte.

2.6. Segment annotation

Each image segment on a superpixel was annotated with the support of a fishery engineering expert with technical knowledge of fish reproduction, thus creating a collection of superpixel references for training and testing the system. As a result of the annotation, 8,578





class	examples	%	qty.
<i>oocyte</i>		4.13	354
<i>dirtiness</i>		7.59	651
<i>dark background</i>		42.22	3.622
<i>light background</i>		46.06	3.951

Fig. 4. Examples of images sliced with SLIC, creating superpixels of set of images divided into classes, and their respective percentages and quantities.

Table 1
Description of attributes extracted from superpixel.

Description	Method	Qty.
<i>Color = 36</i>		
Calculate min, max, mean, and standard deviation for color channels RGB, HSV, and CIELab (Swain and Ballard, 1991)	RGB (red, green, and blue)	12
	HSV (hue, saturation and value)	12
	CieLab (L , a , b)	12
<i>Texture = 214</i>		
Contrast, dissimilarity, homogeneity, asymmetry, energy, and correlation for angles of 0°, 45°, and 90° and distances 1 and 2.	GLCM (gray-level co-occurrence matrix) (Soh et al., 1999)	36
Filters with eight angles (0, 22.5, 45, 67.5, 90, 112.5, 135, 157.5), $\sigma = 1$ and $\sigma = 3$ and 5 frequencies (0.01, 0.1, 0.25, 0.5, 22, 5, 0.9)	Gabor Filter Bank (Feichtinger and Zimmermann, 1998)	160
Histogram with 18 bins calculated with 16 neighbors and equal radius 2.	LBP (local binary patterns) (Van Klaveren et al., 2003)	18
<i>Shape and Gradient = 145</i>		
Set of 7 invariant moments of Hu. Calculate raw and central set of image moments of orders 1 and 2 ($M_{0,1}$, $M_{1,0}$, $M_{1,1}$, $M_{0,2}$, $M_{2,0}$) (Ming-Kuei Hu, 1962)	Moments Hu	7
	Central moments	10
With images of 128-by-128 pixels divided into 4-by-4 blocks. Each block extracts histogram with eight orientations	HOG (histogram of oriented gradients) (Dalal and Triggs, 2005)	128
	Total quantity of attributes	395

Table 2
Results of performance metrics for each class used. Boldfaced results are highest values.

Performance metrics (%)					
Classifier	CCR	Precision	Recall	F-measure	ROC area
SVM	97.19	97.10	97.20	97.00	98.20
Random forest	96.55	96.40	96.50	96.30	99.70
J48	95.47	95.50	95.50	95.50	97.10
k-NN	94.40	93.80	94.40	93.80	95.60
Naive Bayes	90.03	91.90	90.00	90.70	97.20

superpixel images were created, as shown in Fig. 4. These images were distributed among four identification classes with their respective quantities: oocyte = 354, dirtiness = 651, dark background = 3.622, and light background = 3.951. The oocyte and dirtiness classes were recorded in their entirety.

2.7. Attribute extraction and classification

To describe the characteristics of each superpixel, we used 395 attributes, as listed in Table 1. Thirty-six attributes were used to calculate the min, max, mean, and standard deviation in three color channels of red, green and blue (RGB) ($n = 12$), and hue, saturation and value (HSV) ($n = 12$). International Commission on Illumination and L^* for the lightness from black (0) to white (100), a^* from green (−) to red (+), and b^* from blue (−) to yellow (+) CIELab color space information ($n = 12$). Meanwhile, 214 texture characteristics were extracted using a gray level co-occurrence matrix (GLCM) ($n = 36$), Gabor filter (GF) ($n = 160$), and local binary pattern (LBP) ($n = 18$). Finally, the shape and gradient features obtained totaled 145 attributes as Moments Hu ($n = 7$), Central Moments ($n = 10$), and histograms of oriented gradient (HOGs) ($n = 128$).

The characteristics extracted from each superpixel, associated with their respective classes (oocyte, light background, dark background, and dirtiness), were submitted to the following machine learning algorithms: SVM (Platt, 1999), decision trees using the algorithms J48 (Quinlan, 1986) and random forest (Ho, 1995), k-nearest neighbors (k-NN) (Altman, 1992), and Naive Bayes (Russell and Norvig, 2003).

2.8. Experimental setup

Five metrics were used to evaluate the performance of the

classifiers: CCR, precision, recall, F-measure, and ROC area. Tenfold stratified cross-validation was used to randomly split the dataset into training on test sets. In this scheme, the dataset images were divided into 10 folds by ensuring that each fold had the same ratio of each class. Then, a fold was used in a test while the remaining folds were used to train the classifiers. This process was repeated 10 times using each fold exactly one time for the test. Finally, the correct classification rate was given by the average of the 10 rounds. For each algorithm tested, the mean performances of the adjusted metrics for problems with more than two classes were calculated. To verify if the classifiers tested differed statistically in relation to performance, we used a one-way ANOVA hypothesis test performed with the R-Studio statistical software, with each block corresponding to one class problem. The data were also analyzed from a descriptive statistical line using box plots and confusion matrices.

3. Results and discussion

Table 2 presents the results for all performance metrics for each of the five classifiers used: J48, k-NN, Naive Bayes, random forest, and SVM. Considering the results of Table 2, it is verified that the performance indicators present different values for each of the classifiers. Regarding the performance criteria, the largest CCR value was obtained by the SVM classifier, followed by the Random Forest, J48, k-NN, and Naive Bayes classifiers.

Duan et al. (2019) used the Watershed segmentation technique on oocyte images captured by optical microscopy with a Canon EOS 600D camera and applied an automatic visual inspection to identify and count carp eggs (*Cyprinus carpio*). These authors compared human with automatic performance and achieved 100% accuracy using the algorithm. However, in the present research, only cellular camera-captured images were used. This did not have a high image resolution as in the experiment performed by Duan et al. (2019). Nevertheless, we achieved an oocyte recognition of higher than 97%, thus showing the efficiency of oocyte analysis using a cellular device.

The classifier data were analyzed by ANOVA at a significance level of 5% using the F-measure as a metric. A p-value of 0.0623 was obtained. Thus, we have no evidence of a statistically significant difference in the mean performance of the classifiers tested.

Fig. 5 displays a box plot of the performance achieved by each classifier with the range of performance variation. According to Fig. 5, the range of the variance obtained was smaller in the scatter range of the resulting data from the SVM and random forest classifiers. This

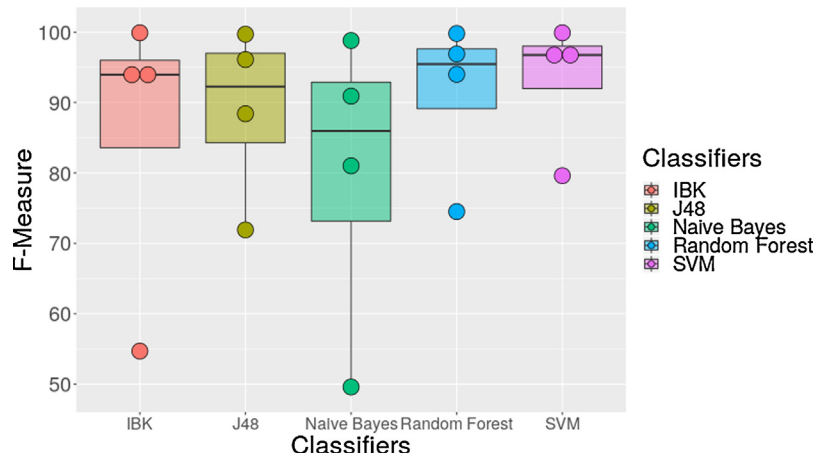


Fig. 5. Box plot comparing performance of classifiers for F -measure metric.

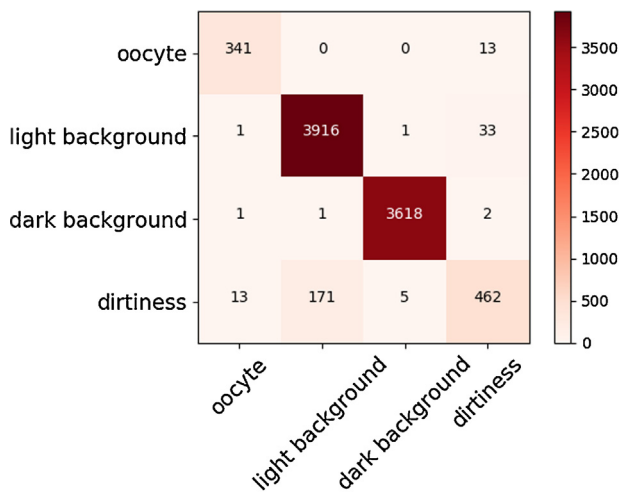


Fig. 6. Confusion matrix diagram obtained by SVM classifier. All correct answers are on main diagonal.

included the analysis of the F -means of the classes.

Fig. 6 presents the confusion matrix of the SVM classifier, which obtained the best result for the classification ratio (CCR). The correct CCR indicates the number of correct decisions by the number of data samples. In this case, we observe in the confusion matrix that the worst accuracy from the classifier SVM occurred between the dirtiness and

light background classes. The SVM classified 171 examples as light background when the correct decision should have been dirtiness. However, 171 examples correspond to only 26% of the total.

Fig. 7 displays a box plot of the classes for the F -measure. Based on the box plot, it is observed that the highest number of errors occur for dirtiness, which also presents a greater variability.

According to Fig. 7, the class dirtiness and light background obtained the highest number of instances classified incorrectly. This is also proven in Fig. 7 because it is the class that has the lowest performance.

Use of the cell phone, which is accessible to a large part of the population, makes aquaculture research quicker and more efficient, as demonstrated in the present research. This is a significant improvement over the situation three decades ago, when acquisition technology was limited to automating the identification and counting of oocytes and fingerlings per image. Research in the 1980s intended to transform the manual labor of oocyte counting in automatic, as described in the work of Withames and Walker (1987). These authors developed a sensor for oocyte counts and obtained a 99.9% accuracy with the device. This value is close to that obtained by this study for the SVM classifier (97.19%).

Considering the available publications, research studies that applied the techniques of computer vision and machine learning also had better accuracy from the SVM classifier, thus corroborating the results presented in this work.

Despite a low number of correct answers, the classification errors indicated that the incorrect classification found was owing to the degree of similarity between these classes. Some dirtiness found was

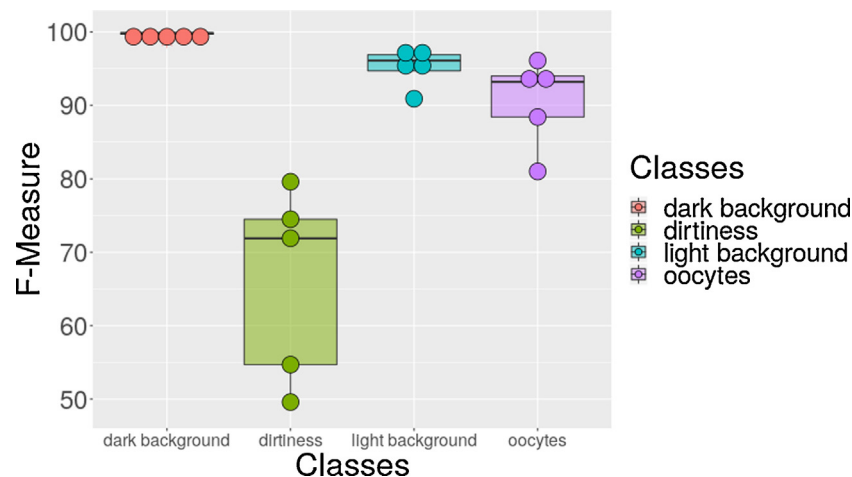


Fig. 7. Box plot comparing performance of classes for F -measure metric.

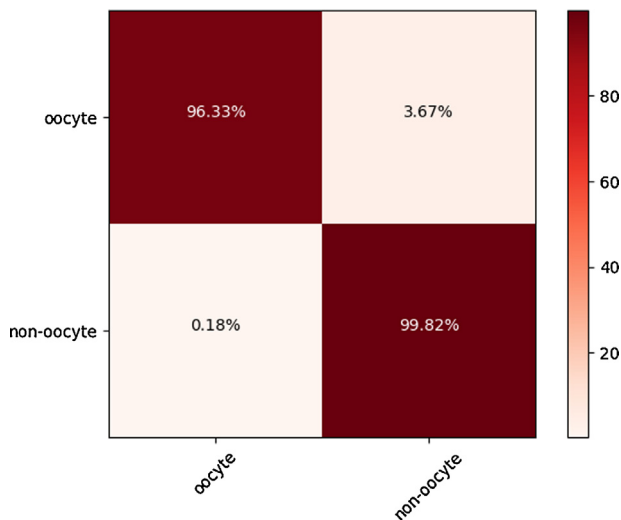


Fig. 8. Normalized confusion matrix of oocyte and non-oocyte classes.

difficult to discriminate from the clear-region area of the Petri dish.

Fig. 8 shows the normalized confusion matrix of the oocyte class and non-oocytes with the percentages of correctness and error. In this case, we consider that the oocyte class achieved a 96.33% true-positive rate. The non-oocyte class, which is the junction of the light background, dark background, and dirtiness classes, confused 0.18%. As the purpose was the oocyte classification, correct answers shown by the normalized confusion matrix support the adopted procedures.

It was necessary to develop a sensitivity regarding the control of the variables and the environment in which the experimentation occurs. An example is acquiring mastery over the possible classes and regions that characterize the collected sample (spawning). The purpose of the paper was to classify and count oocytes. However, we defined three classes (dirtiness, dark background, and light background) to represent “non-oocytes” so that the classifiers fit better. Finally, we presented results using only two classes (oocytes and non-oocytes). This proved to be relevant to the final result of the work.

We consider that the dirtiness class has a mostly light-colored appearance in its area. This matches the results, whereas the confusion between the dirtiness and light background classes does not interfere with the oocyte count.

Because we are using attribute extractors, the risk of overfitting is much lower than in, for example, deep learning methods. In addition, the average accuracy in the training set was 99.89%, while the average accuracy in the test set was 97.20%. Therefore, this difference was only 2.69%, which indicates a low risk of overfitting. Our image bank learned how to identify what is not an oocyte, as the light and dark background classes taught this well. This research demonstrated the feasibility of using digital images acquired by cellular devices in oocyte counting. The most important result of this technology is an increase in the number of breeding sites of the most diverse fish for ornamental use and (mainly) food. This is because once human beings noticed that aquatic life is limited to attend the human population growth, research in this area increased. The entire fish production chain depends on the viability of gametic cells, according to Lubzens et al. (2017), and the technologies that use computer vision aid in the control of oocyte production, identification, and quantification (see Duan et al., 2015) fingerlings and fish.

4. Conclusions

In this article, we proposed a new approach based on a SLIC segmentation method to count lambari oocytes using images obtained at a distance of 10 cm above the target by a smartphone. We considered a

step of segmentation of the Petri dish image to detect oocytes captured with smartphones by considering a K-value equal to 16,000. Next, a feature extraction step was performed using visual descriptors including color, gradient, texture, and shape. The correct classification rate confirmed that our approach obtained an accuracy of 97.19% in lambari oocyte classification using the SVM classifier.

Few studies have been carried out using computerized vision and supervised learning in aquaculture. No studies were found in the literature that used a smartphone to obtain images of oocyte collection in real time. Studies using technologies in the area of fish reproduction have been scarce owing to the biological complexity involved. In many breeding attempts, success is not achieved owing to the sensitivity of oocytes and sperm. As part of our future work, we intend to carry out new experiments with other species of fish and other models of higher-resolution smartphones and in controlled environments.

Using recent approaches to deep neural networks, we intend to apply more state-of-the-art methods such as deep neural networks with regional object recognition (region-based convolutional neural networks (R-CNN), you only look once (YOLO), single shot detector (SSD) or MobileNet) and compare the results with those obtained in this article.

Acknowledgements

Some of the authors were awarded scholarships from the Brazilian National Council of Technological and Scientific Development (CNPq), the Coordination for the Improvement of Higher Education Personnel (CAPES), and the technical-scientific cooperation institutional between the Federal Institute of Education Science and Technology of Mato Grosso do Sul and Dom Bosco Catholic University. We would like to thank Editage (www.editage.com) for English language editing. Additional support was received from the Foundation for the Support and Development of Education, Science and Technology in the State of Mato Grosso do Sul (FUNDECT).

References

- Achanta, R., Shaji, A., Smith, K., Lucchi, A., Fua, P., Süsstrunk, S., 2012. SLIC superpixels compared to state-of-the-art superpixel methods. *IEEE Trans. Pattern Anal. Mach. Intell.* 34 (11), 2274–2282. <https://doi.org/10.1109/TPAMI.2012.120>.
- Altman, N.S., 1992. An introduction to kernel and nearest-neighbor nonparametric regression. *Am. Stat.* 46 (3), 175–185. <https://doi.org/10.1080/00031305.1992.10475879>.
- Bittencourt, F., Damasceno, D.Z., Diemer, O., Boscolo, W.R., Feiden, A., Romagosa, E., 2018. The effects of L-lysine in the diet of silver catfish (*Rhamdia voulezi*) female broodstocks. *Latin Am. J. Aquat. Res.* 46 (1), 1–11. <https://doi.org/10.3856/vol46-issue1-fulltext-x>.
- Dalal, N., Triggs, B., 2005. Histograms of oriented gradients for human detection. In: Schmid, C., Soatto, S., Tomasi, C. (Eds.), *International Conference on Computer Vision & Pattern Recognition (CVPR'05)*, Vol. 1. IEEE Computer Society, San Diego, United States, pp. 886–893. <https://doi.org/10.1109/CVPR.2005.177>.
- Duan, Y., Stien, L.H., Thorsen, A., Sandlund, N., Li, D., Fu, Z., Meier, S., 2015. An automatic counting system for transparent pelagic fish eggs based on computer vision. *Aquacult. Eng.* 67, 8–13. <https://doi.org/10.1016/j.aquaeng.2015.05.001>.
- Duan, Y., Li, D., Stien, L.H., Fu, Z., Wright, D.W., Gao, Y., 2019. Automatic segmentation method for live fish eggs microscopic image analysis. *Aquacult. Eng.* <https://doi.org/10.1016/j.aquaeng.2019.01.004>.
- FAO, 2018. The State of World Fisheries and Aquaculture 2018 – Meeting the Sustainable Development Goals, Vol. 47. Food & Agriculture Org. <http://www.fao.org/3/i9540en/i9540EN.pdf>.
- Feichtinger, H., Zimmermann, G., 1998. Gabor Analysis and Algorithms. pp. 123–170. https://doi.org/10.1007/978-1-4612-2016-9_4.
- Ganias, K., 2013. Determining the indeterminate: evolving concepts and methods on the assessment of the fecundity pattern of fishes. *Fish. Res.* 138, 23–30. <https://doi.org/10.1016/j.fishres.2012.05.006>.
- Gong, A., Yu, J., He, Y., Qiu, Z., 2013. Citrus yield estimation based on images processed by an android mobile phone. *Biosyst. Eng.* 115 (2), 162–170. <https://doi.org/10.1016/j.biosystemseng.2013.03.009>.
- Hall, M., Frank, E., Holmes, G., Pfahringer, B., Reutemann, P., Witten, I.H., 2009. The WEKA data mining software. *ACM SIGKDD Explor. Newslett.* 11 (1), 10. <https://doi.org/10.1145/1656274.1656278>.
- Ho, T.K., 1995. Random decision forests. *Proceedings of the Third International Conference on Document Analysis and Recognition, ICDAR'95*. IEEE Computer Society, Washington, DC, USA, pp. 278–285. <http://dl.acm.org/citation.cfm?id=>

- 844379.844681.
- Kirchner, R.M., Chaves, M.A.D., Silinske, J., Essi, L., Durigon, E.G., Scherer, M.E., Durigon, E.G., 2016. Análise da produção e comercialização do pescado no Brasil. *Rev. Agro@mbiente On-line* 10 (2), 168. <https://doi.org/10.18227/1982-8470ragro.v10i2.2783>.
- Lubzens, E., Bobe, J., Young, G., Sullivan, C.V., 2017. Maternal investment in fish oocytes and eggs: the molecular cargo and its contributions to fertility and early development. *Aquaculture* 472, 107–143. <https://doi.org/10.1016/j.aquaculture.2016.10.029>.
- Ming-Kuei Hu, 1962. Visual pattern recognition by moment invariants. *IEEE Trans. Inform. Theory* 8 (2), 179–187. <https://doi.org/10.1109/TIT.1962.1057692>.
- Parashar, A., Parashar, A., 2017. Importance of computer vision for human life. *Int. J. Adv. Res.* 5 (3), 2396–2399. <https://doi.org/10.21474/IJAR01/3769>.
- Platt, J.C., 1999. *Advances in Kernel Methods*. MIT Press, Cambridge, MA, USA, pp. 185–208. Ch. Fast Training of Support Vector Machines Using Sequential Minimal Optimization. <http://dl.acm.org/citation.cfm?id=299094.299105>.
- Quinlan, J.R., 1986. Induction of decision trees. *Mach. Learn.* 1 (1), 81–106. <https://doi.org/10.1023/A:1022643204877>.
- Russell, S.J., Norvig, P., 2003. *Artificial Intelligence: A Modern Approach*, 2nd ed. Pearson Education.
- Santinón, J.J., Hernández, D.R., Sánchez, S., Domitrovic, H.A., 2010. Duração da larvicultura sobre o desempenho posterior de juvenis de jundiá, *Rhamdia quelen*, criados em tanques-rede. *Ciência Rural* 40 (5), 1180–1185. <https://doi.org/10.1590/S0103-84782010005000077>.
- Shimoda, E., Andrade, D.R., Vidal, M.V., Godinho, H.P., Yasui, G.S., 2007. Determinação da razão ótima de espermatozoides por ovócitos de piabanha *Brycon insignis* (pisces - characidae). *Arq. Bras. Med. Vet. Zootec.* 59 (4), 877–882. <https://doi.org/10.1590/S0102-09352007000400009>.
- Singh, S., Kumar, V., 2016. DimensionApp: Android App to Estimate Object Dimensions. pp. 3–5. [arXiv:1609.07597](https://arxiv.org/abs/1609.07597).
- Soh, L.-k., Tsatsoulis, C., Member, S., 1999. Texture analysis of SAR sea ice imagery. *IEEE Trans. Geosci. Rem. Sens.* 37 (2), 780–795. <https://doi.org/10.1109/36.752194>.
- Swain, M.J., Ballard, D.H., 1991. Color indexing – Springer. *Int. J. Comput. Vis.* 7 (1), 11–32. <https://link.springer.com/content/pdf/10.1007%2FBF00130487.pdf>.
- UNDP, 2015. Human Development Report 2015 Work for Human Development. United Nations Development Programme. http://hdr.undp.org/sites/default/files/2015_human_development_report_1.pdf.
- Van Klaveren, E.P., Michels, J.P.J., Schouten, J.A., 2003. The orientational and structural properties of N2 and N2-AR solids, high pressure. *Int. J. Mod. Phys. C* 10 (2), 445–453. <https://doi.org/10.1142/s0129183199000334>.
- Withames, P.R., Walker, M.G., 1987. An automated method for counting and sizing fish eggs. *J. Fish Biol.* 30 (3), 225–235. <https://doi.org/10.1111/j.1095-8649.1987.tb05748.x>.
- Zhang, X., Zhang, Y., Yang, T., Yang, Y.-H., 2017. Synthetic aperture photography using a moving camera-IMU system. *Pattern Recogn.* 62, 175–188. <https://doi.org/10.1016/j.patcog.2016.07.019>.